

Computational design of Si/SiO₂ interfaces: Stress and strain on the atomic scale

Anatoli Korkin*

Nano & Giga Solutions, Gilbert, Arizona 85296, USA

J. C. Greer

Tyndall National Institute, Cork, Ireland

Gennadi Bersuker

SEMATECH, Austin, Texas 78741, USA

Valentin V. Karasiev and Rodney J. Bartlett

Quantum Theory Project, University of Florida, Gainesville, Florida 32611, USA

(Received 23 August 2005; revised manuscript received 13 January 2006; published 12 April 2006)

In this paper, we present results of a comparative computational study of silicon oxide interfaces with (100), (111), and (110) silicon surfaces. Density functional theory (DFT) in the local density approximation (LDA) and generalized gradient approximation with plane wave basis set and in the LDA approximation with localized numerical atomic orbitals are applied to investigate the relation between the structure and topology of chemical bonds and stress and strain effects at different Si-SiO₂ interfaces, which play a crucial role in electronics materials and devices. The resulting stress energies are discussed in terms of chemical, mechanical, and electric polarization components. According to our observations, chemical and mechanical components in the interface energy are not sufficient for description of silicon suboxide systems including Si-SiO₂ interfaces and the long range electrostatic interactions provide a non-negligible contribution. We uncovered computationally an effect of thermodynamic stabilization of oxygen incorporation in silicon lattice, which may have potential implications for nanoscale electronic device design. The trends in the stress energies derived from the results of the calculations are independent from the DFT approaches applied in this study.

DOI: [10.1103/PhysRevB.73.165312](https://doi.org/10.1103/PhysRevB.73.165312)

PACS number(s): 68.35.-p, 71.15.Mb, 68.65.Hb, 68.47.Fg

I. INTRODUCTION

The interest and demand for knowledge of the atomic scale structure of Si-SiO₂ interfaces grows as the size of electronic devices shrinks into the nanoscale dimension (<100 nm). Whether the roots of motivation come from the efforts to extend the life of complementary metal-oxide-semiconductor (CMOS) technology or from development of an alternative or hybrid technology, atomic scale insight into the materials and interfaces structures is nowadays becoming mandatory to maintain the current speed of information technology (IT) growth prescribed by the International Technology Roadmap for Semiconductors and Moore's laws (see Ref. 1 and papers cited therein). Although "technology mining" for new materials to cure the scaling limits of CMOS devices and "treasure hunting" for molecular electronics have nowadays expanded across the entire periodic system, silicon and silicon oxide based materials, interfaces and devices remain the focus of current and future electronics and photonics.

The unique properties of the Si-SiO₂ interface and recipes for its extremely high precision growth are well known in the semiconductor industry, although the underlying chemistry and physics laws are not always well understood at a fundamental atomic scale level (see, for example, Refs. 2–4, and the literature cited therein). Moreover, nanoscale dimensions in thin films [one-dimensional (1D) nanoscale], nanowires [two-dimensional (2D) nanoscale], and quantum dots [three-dimensional (3D) nanoscale] bring new challenges since

many fundamental properties of materials and the corresponding characteristics of devices change *qualitatively* with only a few atoms located in the direction of electron, photon, or phonon propagation. Development of quantum mechanical methods, their high-level implementation into computer programs, and the growing power of computers permit studying materials properties theoretically, thus introducing computational atomic scale design as a new approach in materials science, complimentary to, or even as an alternative to costly experiments.

Design of an interface between two materials either experimentally or computationally requires a selection of the surface and termination of the substrate materials. Figure 1 shows the fragments of unreconstructed (100), (111), and (110) silicon surfaces. The density of the atoms on the silicon surface increases in the order: (100) < (111) < (110) in the

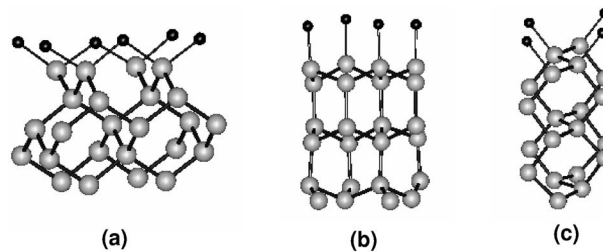


FIG. 1. Fragments of unreconstructed silicon surfaces with the missing silicon atoms shown as the small black circles: (a) (100), (b) (111), (c) (110).

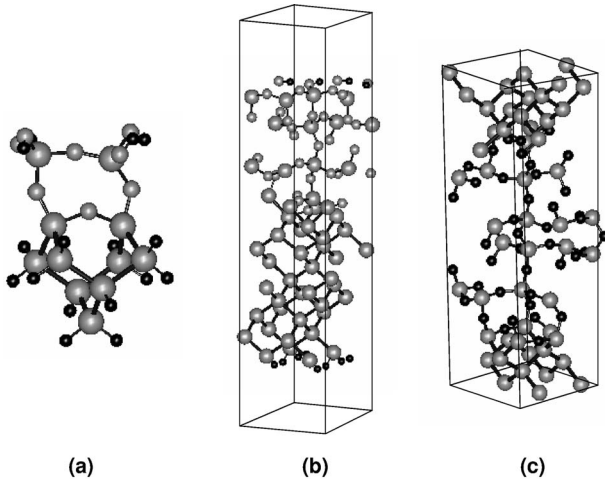


FIG. 2. Models of Si(100)-SiO₂ interface: (a) Si₁₁O₈H₁₆ cluster, (b) 2D periodic slab {Si₅₂O₃₂H₁₂} (see Ref. 20), (c) 3D lattice {Si₅₂O₄₄} (see Ref. 22). Silicon—large grey circles; oxygen—small grey circles, hydrogen—small black circles.

proportion $1:2/\sqrt{3}:\sqrt{2}$. Silicon atoms on the (100) surface tilt to each other by forming “surface dimers,” which leads to the 2×1 surface reconstruction. Further alternative buckling results in (2×2) , (4×2) , and (4×4) reconstructions.^{5–11} The clean (111) surface has well established 7×7 reconstruction,^{12,13} while reconstruction of the (110) surface is less certain and very sensitive to the presence of adatoms.¹⁴

The most technologically relevant surface in microelectronics, Si(100), is also, as a consequence, the most popular one in molecular (cluster) (see, for example, Refs. 15–19) and solid state (periodic) (see, for example, Refs. 20–26) computational studies of Si-SiO₂ interface growth, structure, and properties. Examples of a cluster and 2D and 3D periodic²⁷ models of Si(100)-SiO₂ interface are presented in Fig. 2. Each model has its own advantages and limitations. In order to study adsorption and deposition, a surface/vacuum interface should be present in the cluster [Fig. 2(a)] (implicitly) or in the periodic model [Fig. 2(b)] (explicitly). However these types of models have limited applicability to study stress and strain effects at the interface, since artificial termination (usually by hydrogen atoms) and the small number of atoms in the unit cell or in the cluster create unrealistic mechanical forces and electric polarization. The 3D periodic models [Fig. 2(c)] are better suited to study the stress-strain relations at the interface, although they have the same limitation on the number of atoms. Presence of two similar or equivalent (if the symmetry requirement is imposed) Si-SiO₂ interfaces in the unit cell makes this model also useful for simulation of the real systems containing double Si-SiO₂-Si (e.g., in transistor gate stack) or SiO₂-Si-SiO₂ (e.g., in silicon-on-insulator channel) interface in CMOS and other electronic and photonic devices.

II. COMPUTATIONAL DETAILS

In the present study, we carried out calculations using density functional theory (DFT) in the local density approxi-

mation (LDA)²⁸ and generalized gradient approximation (GGA)^{29–31} with plane wave (PW) and in LDA approximation also with numerical atomic orbitals (NAO) basis sets as implemented in the VASP³² and SIESTA³³ programs, respectively. Core electrons were replaced by the norm-conserving pseudopotentials³⁴ in the Troullier-Martins (TM) form³⁵ in the NAO basis set calculations and by the ultrasoft pseudopotentials^{36,37} in PW calculations. The PW basis set was truncated by the 396 eV energy and 700 eV augmentation charge cutoffs. The Si-SiO₂ interface and the reference Si and SiO₂ supercells have been selected in a way that they have a similar number of atoms and the cell dimensions. Our previous study of the convergence criteria³⁸ has demonstrated that the relaxation of the SiO_x periodic systems with $2 \times 2 \times 1k$ points and standard force and density matrix convergence criteria implemented in VASP³² provide sufficient *chemical* accuracy (bond length error less than 0.01 Å and energy error in the reaction type equations about or less than 0.1 eV) with *a* and *b* unit cell parameters larger than 5 Å and *c* parameter larger than 10 Å in the studied interface and reference periodic supercells. The double zeta plus polarization (DZ+P) basis set was used in the NAO calculations along with the 100 Ry mesh cutoff (equivalent plane wave energy cutoff for the grid) and 0.04 eV/Å force convergence threshold in the unit cell and ion relaxation. Although the results of the calculations with both PW and NAO calculations converge with the increased number of basis set functions, computational studies of the large systems are limited by the computational power. Advantages and deficiencies of DFT methods based on limited PW and NAO basis sets are generally known. However, DFT studies with both plane wave and localized atomic orbital (AO) used in the same paper are relatively rare, while the systems, which include an interface between two materials of the different type (polar and nonpolar covalent bonding) in the periodic lattice, are of clear interest for a comparative study using both types of basis set functions.

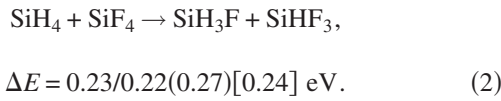
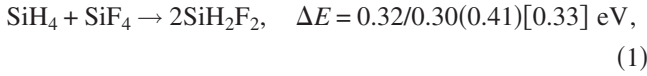
The Si-SiO₂ interfaces, which have been constructed and studied in this paper, are in the range of 88 to 112 atoms in the unit cell. The unit cell length normal to the interfaces ranges from 24 to 40 Å, while the unit cell lengths parallel to the interfaces are in the range of 5.5 to 8 Å. As the reference systems for calculation of the interface stress, we computed comparably sized 96-atom tetragonal supercells of Si, 72-atom orthorhombic supercells of α - and β -quartz, and 96-atoms tetragonal supercells of α - and β -cristobalite. The SiO₂ and Si 96-atom supercells were tested in our previous study³⁸ for energy convergence with respect to *k* point sampling using a uniform grid of *k* points as suggested by Monkhorst and Pack.³⁹ Convergence within 0.1 eV was achieved with a $2 \times 2 \times 1k$ point mesh and this level of *k* point sampling is used for all energies reported in the present study. We also computed comparatively the unit cells of α - and β -quartz (9 atoms, hexagonal) and α - (12 atoms, tetragonal) and β -cristobalite (24 atoms, cubic) with $4 \times 4 \times 4k$ point mesh in different approximations (see details below) and tested selected structures for convergence with $6 \times 6 \times 6k$ point mesh, which demonstrated that the energy convergence is reached with a smaller mesh on the level 0.03 eV for the $4 \times 4 \times 4k$ point mesh.

III. RESULTS AND DISCUSSION

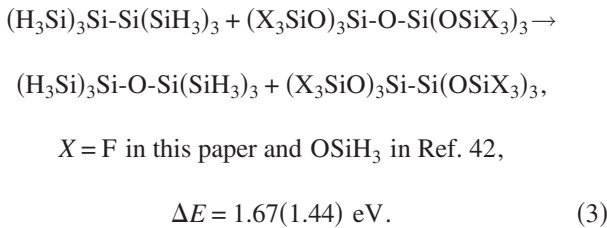
A. Intermediate valence states of silicon

Whether abrupt (thin) or thick, Si-SiO₂ interfaces are characterized by presence of the silicon atoms in the intermediate valence states between zero (bulk silicon) and +4 (bulk silicon dioxide). “Chemical stress” due to the interface formation is revealed by the presence of the intermediate valence states of silicon and can be defined from computation of hypothetical *isodesmic reactions*⁴⁰ between molecules (clusters), which are free from the mechanical stress but balance the number of Si-Si and Si-O bonds for both sides of a reaction equation. This approach is similar to “energy penalties” used to calculate deviations from additive sums of Si-Si and Si-O bond energies in silicon suboxides.^{41,42}

Equations (1) and (2) provide examples of such reactions with silicon in zero and +4 oxidation states on the left hand side and in intermediate valence states on the right hand side of the equations



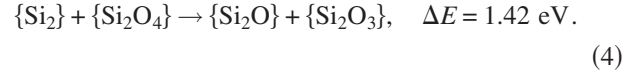
Both reactions are endothermic and results of DFT, LDA, and GGA methods with the NAO basis [first two numbers presented in relations (1) and (2)] are very close and demonstrate good agreement with more sophisticated MP4/6-3+G method⁴³ (in parenthesis), and the most accurate CCSD(T)/cc-pVTZ//CCSD/cc-pVDZ approach⁴⁴ (in the square brackets). A larger endothermic energy has been obtained in reaction (3) computed using the DFT LDA approach in our paper ($X=\text{F}$) and with the GGA approach by Bongiorno and Pasquarello ($X=\text{OSiH}_3$)⁴²



In Eq. (3), two Si(+4) and two Si(0) atoms in the left hand side change their oxidation state to +3 and +1, respectively, in the right hand side of equation. F (OSiH₃ in Ref. 42) and H atoms replace terminated bonds in SiO₂ and Si lattice, respectively. The positive (endothermic) energy in Eqs. (1)–(3) demonstrates that formation of the intermediate valence states of silicon from unoxidized Si(0) and completely oxidized Si(+4), used as a reference, is energetically unfavorable. In spite of the differences in the reference systems and DFT methods, our results and those obtained in Ref. 42 are reasonably close.

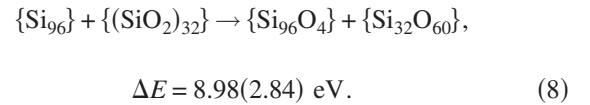
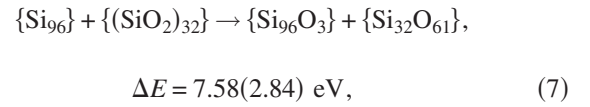
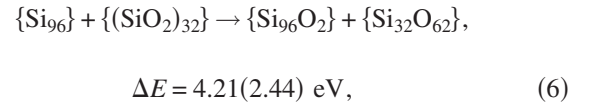
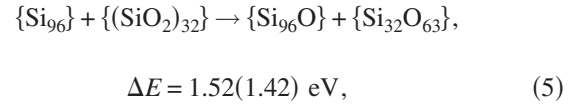
Hamann⁴¹ has computed *energy penalties* for each suboxide silicon state using DFT GGA calculations of the periodic systems constructed from “the diamond Si lattice with an O

placed between each Si pair.” The corresponding energy of the formal reaction of the oxygen atom transfer from SiO₂ into the Si lattice computed in Ref. 41 is close to the one computed with molecular systems in Eq. (3)



Energies in Eqs. (3) and (4) are equal to twice the sum of energy penalties for Si(+1) and Si(+3).^{41,42}

In Eqs. (5)–(8), we present the energies of the subsequent transfer of four oxygen atoms from SiO₂ into the Si periodic systems composed by 96-atom supercells and computed by the GGA PW91 approach with the PW basis

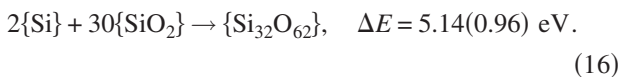
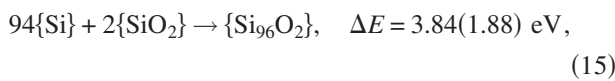
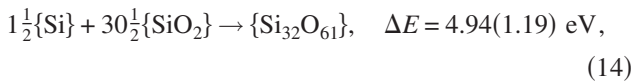
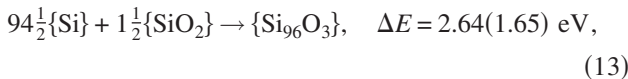
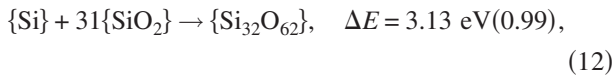
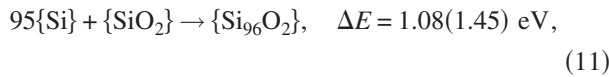
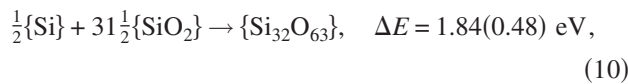
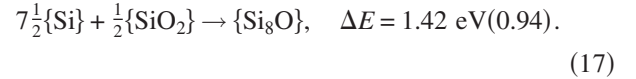
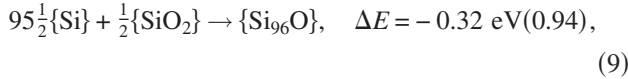


The values in parenthesis [see also Eqs. (9)–(16)] are the penalty energies computed by Hamann.⁴¹ Si and SiO₂ lattices on the left side of Eqs. (5)–(8) were represented by tetragonal supercells composed of 96 atoms, 12 cubic units cells of silicon (2×2×3), and 4 cubic unit cells of β-cristobalite (2×2×1), the most stable SiO₂ at the GGA/PW approach. Four oxygen atoms were subsequently removed from the same SiO₄ tetrahedron in SiO₂ and inserted into the Si-Si bonds of one Si atom in the Si lattice followed by ion positions and unit cell relaxation (energy minimization).

Except for Eq. (5), energies of the oxygen atoms transfer from SiO₂ into Si lattice are substantially larger than the penalty energies computed in Ref. 41 and increase with the number of transferred atoms. The energy in Eq. (5) is close to the penalty energy given in parenthesis. However, the subsequent analysis of the energies [see Eqs. (9)–(16)] of the suboxides in the right side of Eqs. (5)–(8) shows that incorporation of an oxygen atom in {Si₉₆} supercell displays a stabilization effect, while all other {Si_xO_y} systems are thermodynamically unstable with regard to the reference Si and SiO₂. The instability grows with the deviation from both limits, e.g., with the number of oxygen atoms incorporated in the silicon supercell and the number of oxygen vacancies in SiO₂ supercell, reflecting an increasing mechanical stress, e.g., expansion stress originated by vacancies in the oxygen deficient SiO₂ supercells and compression stress originated by oxygen atoms incorporated into the silicon supercell.

TABLE I. Average Si-Si and Si-O bond lengths (in Å), Si-O-Si bond angles (in grads) and the unit volume (in Å³) in the periodic systems in Eqs. (5)–(8).

X	{Si ₃₂ O _{64-x} }				{Si ₉₆ O _x }			
	Si-Si	Si-O	Si-O-Si	V	Si-Si	Si-O	Si-O-Si	V
0		1.632	146.7	1462	2.338			1888
1	2.333	1.637	140.7	1348	2.345	1.644	161.3	1915
2	2.464	1.637	141.3	1352	2.347	1.669	134.0	1924
3	2.418	1.643	135.2	1234	2.350	1.643	145.7	1935
4	2.458	1.641	135.8	1225	2.350	1.678	115.2	1930



The negative energy in Eq. (9) and smaller than penalty energy value in Eq. (11) can be explained by the polarization (electrostatic) energy that resulted from incorporation of the more electronegative oxygen atom in the silicon supercell. In order to check whether this stabilization effect is sensitive to the computational approach, we have calculated the systems in Eq. (9) at the LDA as well and obtained a similar result: -0.25 eV. In contrast to Ref. 41, we did not impose any symmetry constraint in optimization of atom positions and unit cell parameters. However, the size of the supercell is indeed a critical factor for polarization effects and mechanical stress. Incorporation of oxygen atom in the 8-atom Si unit cell followed by unconstrained relaxation of atomic positions and cell parameters has resulted in a positive (endothermic energy) exceeding the penalty energy

The average Si-Si and Si-O bond lengths and Si-O-Si bond angles and the supercell volumes of the periodic {Si_nO_m} systems from the right side of Eqs. (5)–(8) are presented in the Table I. There is no simple correlation between those parameters and the number of oxygen atoms in the system, which is primarily due to the flexibility of the Si-O-Si bond, angles, which can change significantly in response to the modification of the local chemical bonding and van der Waals and electrostatic forces. Note, that {Si₃₂O₆₀} and {Si₉₆O₄} lattices in Eq. (8) and in the last row in Table I (see Fig. 3) denote the models of the smallest defect-free Si-in-SiO₂ and SiO₂-in-Si quantum dots, respectively.

B. Construction of SiO₂-Si lattices

To construct the double-interface Si(100)-SiO₂ lattice, Dharma-Wardana *et al.*²² used a combination of a mirror reflection of the single-interface structure designed by Pasquarello *et al.*²⁰ and subsequent relaxation by energy minimization. We applied a similar approach in order to design the double-interface Si(111)-SiO₂ and Si(110)-SiO₂ supercells. In the Si(100)-SiO₂ interface models described in Refs. 20 and 22 the lateral dimension of the square surface unit cell is equal or close (if relaxed) to the $\sqrt{2}a$, where a is a silicon unit cell parameter. Such a surface unit cell has four

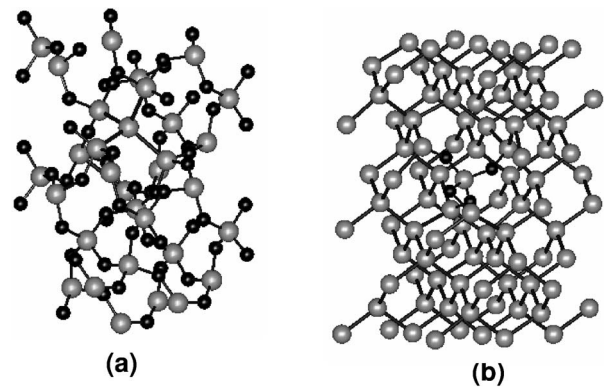


FIG. 3. Models of the smallest defect-free Si-in-SiO₂ and SiO₂-in-Si quantum dots, {Si₃₂O₆₀} (a) and {Si₉₆O₄} (b). Si—large gray circles, O—small black circles.

silicon atoms in it. We have also designed the Si(111)-SiO₂ and Si(110)-SiO₂ interfaces with the same number of (four) silicon surface atoms. The corresponding lateral rectangular surface cell parameters prior relaxation are $\sqrt{2}a \times a$ and $\sqrt{2}a \times \sqrt{3/2}a$, for (110) and (111) surfaces, respectively, which reflects the higher density of the silicon atoms on these two surfaces compared to the (100) surface. After adjusting the unit cell parameters and matching bonding at the interfaces, we have designed initially the single-interface two-layer structures. While β -cristobalite has been used to design Si(100)-SiO₂ interfaces in Refs. 20 and 22, we used α -cristobalite and α -quartz to design interfaces with Si(111) and Si(110) surfaces, respectively, applying the same selection criteria, e.g., better match of the local bonding between two materials at the initial (manual) step of the interface design. However, the subsequent structure relaxation of the flexible SiO₂ framework always leads to the partial amorphization of SiO₂ portion of the supercell, and as it is shown below, our interface structures have similar stress energy to those presented in Ref. 22. Single-interface structures were saturated by hydrogen atoms on both silicon and silicon oxide sides and then relaxed using energy minimization in the DFT LDA approach with constrained lateral dimensions. The vacuum portion of the unit cell allowed relaxation of the slab in the direction perpendicular to the interface. At the next step, we removed the hydrogen atoms and constructed the mirror reflected interfaces, which then were matched at the silicon oxide. Since both (111) and (110) surfaces are symmetric with regard to the Si-SiO₂ interface and we kept the bottom layers of silicon frozen at the first step of relaxation, the silicon atoms at the top and at the bottom of the combined (Si-SiO₂)_{up}-(SiO₂-Si)_{down} unit cell matched automatically at the unit cell translation in a direction perpendicular to the interface. At the final step, the atomic parameters and the unit cell parameters have been relaxed using LDA and GGA methods with PW basis set. All three double-interface Si-SiO₂ unit cells have a similar number of atoms (~ 100) and proportion between Si and SiO₂ components. We have also modified the interface from Ref. 22 by removal of oxygen atoms from surface dimer and backbond position in order to reveal the stress effect of oxygen penetration into the upper silicon layer. The Si-SiO₂ lattices, which have been constructed and computed in this study, are presented in Fig. 4. They are labeled by the number of silicon and oxygen atoms in the supercell and the orientation of the Si substrate. The {Si₅₂O₄₄-100} and {Si₆₈O₄₄-100} superlattices correspond to the structures, FRM1 and FRM2, respectively, described in Ref. 22, which have been designed to reflect experimentally observed distribution of the intermediate silicon oxidation states, Si(+1), Si(+2), and Si(+3). The other models have silicon only in Si(+3) and Si(+1) oxidation states corresponding to SiO₂ and Si portions of the supercells terminated at the interface. According to Ohishi and Hattori, Si(+3) and Si(+1) oxidation states dominate at the interface during oxidation of atomically flat Si(111) surface at the room temperature.⁴⁵

C. Stress and strain in Si-SiO₂ interfaces

In the Si-SiO₂ supercells, which have defect-free interfaces, all silicon atoms are four coordinated and all oxygen

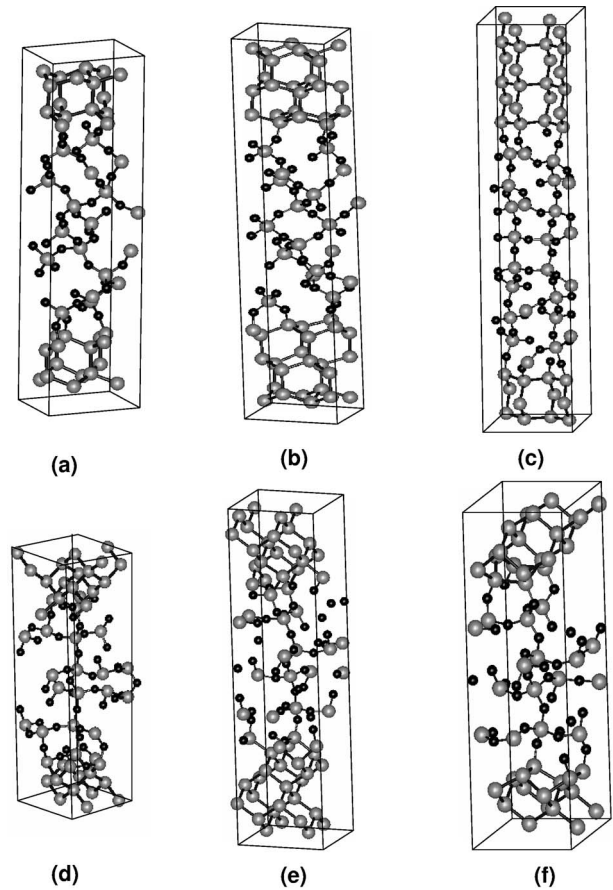
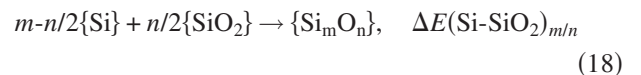


FIG. 4. The structures of Si-SiO₂ interfaces: (a) {Si₅₀O₄₀-111}, (b) {Si₆₆O₄₀-111}, (c) {Si₆₀O₅₂-110}, (d) {Si₅₂O₄₄-100}, (e) {Si₆₈O₄₄-100}, (f) {Si₅₂O₃₆-100}. Si—large gray circles; O—small black circles.

atoms are two coordinated. If the supercell contains m silicon atoms and n oxygen atoms, the total number of Si-Si bonds is equal to $2m-n$ and the number of Si-O bonds is equivalent to $2n$. The same number of Si and O atoms and Si-Si and Si-O bonds exists in the system composed from the separated $(m-n/2)$ Si and $n/2$ SiO₂ units. Thus the energy of formation of the Si-SiO₂ supercell containing m silicon and n oxygen atoms can be defined from the following hypothetical *isodesmic* reaction,⁴⁰ e.g., transformation which preserves the number of bonds of each type



The energy, ΔE , in Eq. (18) can be formally divided into the chemical and mechanical stress of the interface formation and *polarization energy* (long range electrostatic energy effects), which can also contribute to the interface energy. Although intuitively long range electrostatic interactions should provide a non-negligible contribution into the interface energy, developing an additive model for its separation from the mechanical stress (caused by deformation of the bonds and bond angles from their optimal values in nonconstrained systems) is not a simple task and is beyond the scope of this

TABLE II. Relative energies of silica polymorphs (in eV per SiO₂) with regard to α -quartz.

	β -quartz	α -cristobalite	β -cristobalite
GGA PW91/PW	0.01	-0.04	-0.06
GGA PBE/PW	0.02	-0.03	-0.05
GGA RPBE/PW	0.00	-0.06	-0.06
LDA/PW	0.06	0.03	0.02
GGA PBE/NAO	0.03	0.01	0.14
LDA/NAO	0.08	0.08	0.22
LDA/PW ^a	0.02		

^aReference 51.

paper. The *chemical stress* at the interface is affiliated with silicon atoms which have intermediate oxidation between zero (in bulk silicon) and +4 (in bulk SiO₂) (see Sec. III A) and *mechanical stress* appears from the unit cells mismatch and local bonding mismatch in the supercell construction from the crystalline Si and SiO₂ parts. The latter one causes the deformation of bonds and bond angles at the interface relative to their equilibrium values.

The stress energy computed in Eq. (18) depends on the choice of the reference systems, Si and SiO₂, in the left side of the equation. Since the silicon part of the supercell is built from the crystalline silicon, it is natural to use the diamond Si as a reference system for silicon. Selection of the reference for SiO₂ is less straightforward since we have used the different crystalline forms of SiO₂ to design the interfaces with (100) (β -cristobalite), (110) (α -quartz), and (111) (β -cristobalite) surfaces. α -quartz is the most stable form of silica, but the energy difference between quartz and cristobalite is very small (0.03 eV)⁴⁶ and the correct energetic order of different silica polymorphs remains a challenge for the DFT calculation even with the large basis set and high computational thresholds (see, for example, Refs. 47 and 48 and the literature cited therein). The relative energies of four silica polymorphs computed with different DFT approaches are presented in Table II. Although the GGA approach is generally more accurate than LDA, all three GGA flavors with PW basis set show β -cristobalite as a lowest energy structure, while LDA/PW calculations demonstrate lower energy for α -quartz. This result does not change with the larger number of k points and higher plane wave energy cutoff. However, both GGA and LDA methods with NAO basis set

display α -quartz as the lowest energy form. The relaxed parameters of the cubic silicon and β -cristobalite unit cells are 5.446 (5.381) Å and 7.126 (6.8882) Å in GGA (LDA) calculations, respectively [experiment: 5.431 Å for Si (Ref. 49) and 7.166 Å for SiO₂ (Ref. 50)]. The computed value of the unit cell parameters for Si and SiO₂ are closer to the experimental values in GGA calculations with Si unit cell slightly smaller and SiO₂ lattice parameters slightly larger than the experimental values, while LDA calculations result in smaller unit cell dimensions and a larger deviation from the experimental results.

Table III presents the interface stress energies computed using Eq. (18) and the unit cell parameters for the Si-SiO₂ lattices. For the reference SiO₂ systems in the left side of Eq. (18), we used the lowest energy polymorphs, e.g., α -quartz in LDA and β -cristobalite in GGA PW91 calculations with the PW basis set. The relaxed parameters of the silicon lattice (5.446 Å in GGA and 5.381 Å in LDA calculations, respectively) correspond to the surface cell parameters: 7.702 × 7.702 (7.632 × 7.610) for (100) surface, 7.702 × 6.670 (7.610 × 6.590) for (111) surface, and 7.702 × 5.446 (7.610 × 5.381) for (110) surface. According to these surface cell parameters, silicon has a tensile strain on the Si(100)-SiO₂ and on the Si(111)-SiO₂ interface. The situation with Si(110)-SiO₂ is more complex. It shows tensile strain in GGA calculations and deformation strain in the LDA results. Although stress energy can be formally related to the misfit of unit cell parameters of both materials, silicon oxide is much softer material and undergoes partial amorphization (within periodic supercell boundaries) during the parameter relaxation procedure in two step interface supercell design (see Sec. III B).

Among three Si(100)-SiO₂ interfaces the amount of stress is increased with the size of the supercell. The {Si₅₂O₃₆-100} lattice differs from {Si₅₂O₄₄-100} and {Si₆₈O₄₄-100} lattices although by the interface topology: Incorporation of the oxygen atoms in the surface dimer and the backbond in {Si₅₂O₄₄-100} and {Si₆₈O₄₄-100} interfaces adds stress in the silicon lattice (see Fig. 5). Adding two silicon monolayers in the Si(100)-SiO₂ (rows 4 and 5 in the Table III) and the Si(111)-SiO₂ (rows 1 and 2 in the Table I) increase the total stress energy in the supercells by ~0.4 eV and ~0.9 eV, respectively.

GGA and LDA calculations provide similar stress energies for all three types of the interfaces and show the same qualitative trends with regard to the increasing of the number

TABLE III. Lattice stress energies (in eV) in Si-SiO₂ interfaces computed from Eq. (18) and lattice cell parameters (in parenthesis, in angstroms).

Lattice	GGA PW91/PW	LDA/PW
{Si ₅₀ O ₄₀ -111}	9.64(7.443 × 6.529 × 29.63)	9.08(7.334 × 6.439 × 29.13)
{Si ₆₆ O ₄₀ -111}	10.52(7.509 × 6.487 × 35.89)	9.88(7.382 × 6.466 × 35.35)
{Si ₆₀ O ₅₂ -110}	10.01(7.871 × 5.552 × 38.97)	8.88(7.530 × 5.465 × 38.40)
{Si ₅₂ O ₄₄ -100}	10.78(8.009 × 8.023 × 24.46)	11.12(7.873 × 7.884 × 24.21)
{Si ₆₈ O ₄₄ -100}	11.19(7.888 × 7.890 × 30.01)	11.58(7.765 × 7.767 × 29.63)
{Si ₅₂ O ₃₆ -100}	8.58(7.834 × 7.857 × 24.13)	9.00(7.691 × 7.716 × 23.88)

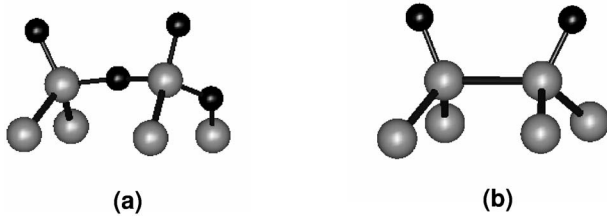


FIG. 5. Fragments of the Si(100)-SiO₂ interfaces: (a) (100)-52/44 and (100)-68/44, (b) (100)-52/36.

of silicon layers (e.g., {Si₅₂O₄₄-100} vs {Si₆₈O₄₄-100} and {Si₅₀O₄₀-111} vs {Si₆₆O₄₀-111}) and modification of the interface composition (e.g., {Si₅₂O₄₄-100} vs {Si₅₂O₃₆-100}). The maximum difference in the stress energies computed with GGA and LDA approaches is 1.13 eV for the {Si₆₀O₅₂-100} superlattice. The stress energies computed using GGA approach are larger than LDA values for S(100)-SiO₂ interfaces and smaller for Si(111)- and Si(110)-SiO₂ interfaces.

Bongiorno and Pasquarello⁴² have estimated mechanical stress at the interface by subtracting chemical stress [sum of energy penalties for the corresponding number of Si(+1), Si(+2), and Si(+3) atoms] from the total stress energy. Although we believe that the polarization energy component in the total interface energy must also be accounted for, a simple model which separates the chemical stress from the remaining stress energy also provides useful information for estimation of the overall stability of the interface. Separation of the total stress energy into additive components depend on the choice of the reference system and the accuracy of the computational approach. We can estimate chemical stress in the Si-SiO₂ superlattices computed in this paper (Fig. 4 and Table III) using penalty energies from Ref. 41 (which are very similar to the corresponding values in Ref. 42). Each supercell has two Si-SiO₂ interfaces. The {Si₅₂O₄₄-100} and {Si₆₈O₄₄-100} supercells (corresponding to FRM1 and FRM2 in the Ref. 22, respectively) have six Si(+3), two Si(+2), and two Si(+1) atoms at each of the two symmetric interfaces in the supercells resulting in 6.80 eV for the chemical stress energy. The remaining supercells have four Si(+3) and four Si(+1) atoms for each interface resulting to 5.68 eV chemical stress energy. All interface energies in Table III are larger than chemical stress estimated above from the energy penalties, thus demonstrating that the sums of mechanical stress

and polarization energy are positive and comparable to the value of the chemical stress.⁴²

Table IV presents the average values and the standard deviations of the bond lengths and bond angles in Si-SiO₂ lattices. In the relaxed Si supercell, Si-Si bond length and Si-Si-Si angle are equal to 2.357 Å and 109.47°, respectively, and in the relaxed SiO₂ supercell the Si-O bond length and O-Si-O and Si-O-Si angles are equal to 1.615 Å, 109.47°, and 141.6°, respectively. Si-Si bond lengths are shorter in Si(111)-SiO₂ lattices and longer than in Si(100)-SiO₂ and Si(110)-SiO₂ lattices than the relaxed value in the silicon lattice, while Si-O bonds are longer than in SiO₂ for all interfaces. The latter results from the fact that Si-O bonds at the intermediate valence states at the interfaces are longer than the bulk values.

IV. CONCLUDING REMARKS

In our paper, we have designed and optimized the novel defect-free Si(111)-SiO₂ and Si(110)-SiO₂ interfaces using the DFT GGA and LDA approaches. We have computed the stress energy for the Si(100)-SiO₂, Si(111)-SiO₂, and Si(110)-SiO₂ superlattices using energies of Si and SiO₂ lattices as a reference. Si(111)-SiO₂ and Si(110)-SiO₂ superlattices designed in this work reveal similar stress energies compared to the Si(100)-SiO₂ presented earlier in the literature.²² Computations with GGA and LDA approaches reveal similar trends in the stress energies in response to increasing the number of silicon layers in the supercell and chemical modification of the interfacial layer.

Energies of hypothetical isodesmic reactions of oxygen atoms transfer from SiO₂ (oxygen vacancy formation) into Si (silicon oxidation) in molecular (cluster) and periodic models help to reveal the nature of the stress at the interface and define it in terms of chemical (intermediate valence state formation) and remaining stress from the local mechanical deformation (deviation from the optimal bond lengths and bond angles) and polarization (charge transfer and Coulomb interaction) energy.

We observed computationally an effect of thermodynamic stabilization of oxygen incorporation into the silicon lattice [see Eqs. (9) and (11)]. This effect depends on oxygen concentration (size of the Si supercell in periodic calculations) and may have potential implication for nanoscale electronic devices, such as quantum dots and wires. It can also be re-

TABLE IV. The average bond lengths and angles and their standard deviations in Si-SiO₂ lattices.^a

Lattice	Si-Si	Si-O	Si-Si-Si	Si-Si-O	O-Si-O	Si-O-Si
{Si ₅₀ O ₄₀ -111}	2.345(33)	1.639(25)	109.2(4.9)	110.9(11.2)	109.5(6.1)	144.6(12.5)
{Si ₆₆ O ₄₀ -111}	2.316(31)	1.634(23)	109.2(5.1)	111.6(10.5)	109.5(5.8)	142.6(13.4)
{Si ₆₀ O ₅₂ -110}	2.376(34)	1.623(18)	109.6(4.4)	107.8(11.9)	109.5(3.4)	141.2(13.7)
{Si ₅₂ O ₄₄ -100}	2.387(37)	1.624(23)	109.6(5.3)	109.5(8.2)	109.2(3.7)	143.1(16.0)
{Si ₆₈ O ₄₄ -100}	2.373(28)	1.622(24)	109.5(4.0)	110.0(8.7)	109.2(4.3)	139.3(15.3)
{Si ₅₂ O ₃₆ -100}	2.402(42)	1.621(29)	109.0(5.7)	111.9(4.7)	109.5(4.6)	135.7(11.6)

^aBonds are presented in angstroms and angles in degrees. The standard deviations for bond lengths are presented in angstroms multiplied by 1000.

lated to the properties of the intermediate SiO₂ layer, which forms at the deposition of the transition metal oxide on silicon (high dielectric) and displays a higher than bulk SiO₂ dielectric constant, which is characteristic for an *oxygen deficient* silicon oxide.⁵² However, the balance of the kinetic and thermodynamic factors (e.g., metastability and true thermodynamic stability) has not been well clarified in the multilayer gate dielectric films on the silicon substrate and the (meta)stability of silicon suboxides at the atomic scale and nanoscale certainly merits further investigation.

ACKNOWLEDGMENTS

This work has been supported by a Science Foundation Ireland Investigator Award and the National Science Foundation Grant No. ITR 0325553. We are grateful to A. Pasquarello and M. W. C. Dharma-Wardana for providing the structures of the interface models to us and to Z. Chen for his kind assistance with computational results for the reference molecular systems. We thank T. Frauenheim for useful discussions.

*Corresponding author. Electronic address: korkin@nanoandgiga.com

- ¹P. M. Zeitzoff, J. M. Hutchby, G. Bersuker, and H. R. Huff, in *Nano and Giga Challenges in Microelectronics*, edited by J. Greer, A. Korkin, and J. Labanowski (Elsevier, Amsterdam, 2003), p. 1.
- ²S. T. Pantelidis and M. Long, *The Physics of SiO₂ and its Interfaces* (Pergamon, New York, 1978).
- ³*Fundamental Aspects of Ultrathin Dielectrics on Si-based Devices*, edited by E. Garfunkel, E. Gusev, and A. Vul', NATO Science Series Vol. 47 (Kluwer Academic Publishers, Dordrecht, 1998).
- ⁴*Fundamental Aspects of Silicon Oxidation*, edited by Y. J. Chabal (Springer, Berlin, 2001).
- ⁵T. D. Poppendick, T. C. Ngoe, and M. B. Webb, *Surf. Sci.* **75**, 287 (1978).
- ⁶W. S. Yang, F. Jona, and P. M. Markus, *Phys. Rev. B* **28**, 2049 (1983).
- ⁷B. W. Holland, C. B. Duke, and A. Paton, *Surf. Sci.* **140**, L267 (1984).
- ⁸N. Jedrecy, M. Sauvage-Simkin, R. Pinchaux, J. Massies, N. Greiser, and V. H. Etgens, *Surf. Sci.* **230**, 197 (1990).
- ⁹D. Badt, H. Wengelnik, and H. Neddermeyer, *J. Vac. Sci. Technol. B* **12**, 2015 (1994).
- ¹⁰E. L. Bullock, R. Gunnella, L. Patthey, T. Abukawa, S. Kono, C. R. Natoli, and L. S. O. Johansson, *Phys. Rev. Lett.* **74**, 2756 (1995).
- ¹¹R. Felici, I. K. Robinson, C. Ottaviani, P. Imperatori, P. Eng, and P. Perfetti, *Surf. Sci.* **375**, 55 (1997).
- ¹²F. J. Giessibl, *Science* **260**, 67 (1995).
- ¹³S. Kitamura and M. Iwatsuki, *Jpn. J. Appl. Phys., Part 2* **35**, L668 (1996).
- ¹⁴M. Menon, N. N. Lathiotakis, and A. N. Andriotis, *Phys. Rev. B* **56**, 1412 (1997).
- ¹⁵A. Markovits and C. Minot, in *Fundamental Aspects of Ultrathin Dielectrics on Si-Based Devices*, edited by E. Garfunkel, E. Gusev, and A. Vul', NATO Science Series Vol. 47 (Kluwer Academic Publishers, London, 1989), p. 131.
- ¹⁶T. Watanabe and I. Ohdomari, *Astron. Astrophys., Suppl. Ser.* **237**, 125 (2004).
- ¹⁷M. K. Weldon, K. T. Queeney, A. B. Gurevich, Y. J. Chabal, B. B. Stefanov, and K. Raghavachari, *J. Vac. Sci. Technol. B* **17**, 1795 (1999).
- ¹⁸I. Vasiliev, J. R. Chelikowsky, and R. M. Martin, *Phys. Rev. B* **65**, 121302 (2002).
- ¹⁹S. P. Karna, A. C. Pineda, W. M. Shedd, and B. K. Singaraju,

- Proc.-Electrochem. Soc.* **99**, 161 (1999); S. P. Karna, H. A. Kurtz, W. M. Shedd, R. D. Pugh, and B. K. Singaraju, *IEEE Trans. Nucl. Sci.* **46**, 1544 (1999).
- ²⁰A. Pasquarello, M. S. Hybertsen, and R. Car, *Phys. Rev. Lett.* **74**, 1024 (1995); *Phys. Rev. B* **53**, 10942 (1996); *Appl. Phys. Lett.* **68**, 625 (1996); *Appl. Surf. Sci.* **104/105**, 317 (1996).
- ²¹A. A. Demkov and O. F. Sankey, *Phys. Rev. Lett.* **83**, 2038 (1999); A. A. Demkov, X. Zhang, and D. A. Drabold, *Phys. Rev. B* **64**, 125306 (2001).
- ²²N. Tit and M. W. C. Dharma-Wardana, *J. Appl. Phys.* **86**, 1 (1999); P. Carrier, L. J. Lewis, and M. W. C. Dharma-Wardana, *Phys. Rev. B* **65**, 165339 (2002).
- ²³E. Degoli and S. Ossicinia, *Surf. Sci.* **470**, 32 (2000); *Opt. Mater.* **17**, 95 (2001).
- ²⁴K. Kato, T. Uda, and T. Terakura, *Phys. Rev. Lett.* **80**, 2000 (1998).
- ²⁵T. Akiyama and H. Kageshima, *Appl. Surf. Sci.* **216**, 270 (2003); T. Akiyama, H. Kageshima, and T. Ito, *Jpn. J. Appl. Phys., Part 2* **43**, 7903 (2004).
- ²⁶A. Bongiorno and A. Pasquarello, *J. Phys.: Condens. Matter* **17**, S2051 (2005).
- ²⁷Technically the computational DFT programs require the lattice to be periodic in all three dimensions, which results in using vacuum above the surface inside of the unit cell.
- ²⁸J. P. Perdew and A. Zunger, *Phys. Rev. B* **23**, 5048 (1981).
- ²⁹J. P. Perdew, J. A. Chevary, S. H. Vosko, K. A. Jackson, M. R. Pederson, D. J. Singh, and C. Fiolhais, *Phys. Rev. B* **46**, 6671 (1992); J. P. Perdew and Y. Wang, *Phys. Rev. B* **45**, 13244 (1992).
- ³⁰J. P. Perdew, K. Burke, and M. Ernzerhof, *Phys. Rev. Lett.* **77**, 3865 (1996).
- ³¹B. Hammer, L. B. Hansen, and J. K. Norskov, *Phys. Rev. B* **59**, 7413 (1999).
- ³²Vienna *ab initio* simulation package (VASP), Version 4.4.5, <http://cms.mpi.univie.ac.at/vasp/>. See also G. Kresse and J. Furthmüller, *Comput. Mater. Sci.* **6**, 4136 (1996).
- ³³Spanish Initiative for Electronic Simulations with Thousands of Atoms (SIESTA), Version 1.3, <http://www.uam.es/departamentos/ciencias/fismateriac/siesta/>. See also J. M. Soler, E. Artacho, J. D. Gale, A. García, J. Junquera, P. Ordejón, and D. Sánchez-Portal, *J. Phys.: Condens. Matter* **14**, 2745 (2002).
- ³⁴W. C. Topp and J. J. Hopfield, *Phys. Rev. B* **7**, 1295 (1973).
- ³⁵N. Troullier and J. L. Martins, *Phys. Rev. B* **43**, 1993 (1991).
- ³⁶D. Vanderbilt, *Phys. Rev. B* **41**, 7892 (1990).
- ³⁷G. Kresse and J. Hafner, *J. Phys.: Condens. Matter* **6**, 8245

- (1994).
- ³⁸T. M. Henderson, J. C. Greer, G. Bersuker, A. Korkin, and R. J. Bartlett, in *Defects in Advanced High-k Dielectric Nano-Electronic Semiconductor Devices*, edited by E. Gusev (Springer, Berlin, 2006), p. 373.
- ³⁹H. J. Monkhorst and J. D. Pack, *Phys. Rev. B* **13** 5188 (1976).
- ⁴⁰W. J. Hehre, L. Radom, and P. v. R. Schleyer, *Ab Initio Molecular Orbital Theory* (Wiley, NY, 1986), p. 298.
- ⁴¹D. R. Hamann, *Phys. Rev. B* **61**, 9899 (2000).
- ⁴²A. Bongiorno and A. Pasquarello, *Phys. Rev. B* **62**, R16326 (2000).
- ⁴³H. B. Schlegel, *J. Phys. Chem.* **88**, 6254 (1984).
- ⁴⁴ACES II is a program product of the Quantum Theory Project, University of Florida. Authors: J. F. Stanton, J. Gauss, J. D. Watts, M. Nooijen, N. Oliphant, S. A. Perera, P. G. Szalay, W. J. Lauderdale, S. A. Kucharski, S. R. Gwaltney, S. Beck, A. Balková, D. E. Bernholdt, K. K. Baeck, P. Rozyczko, H. Sekino, C. Hober, and R. J. Bartlett. Integral packages included are VMOL (J. Almlöf and P. R. Taylor); VPROPS (P. Taylor); ABACUS (T. Helgaker, H. J. Aa. Jensen, P. Jørgensen, J. Olsen, and P. R. Taylor).
- ⁴⁵K. Ohishi and T. Hattori, *Jpn. J. Appl. Phys., Part 2* **33**, L675 (1994).
- ⁴⁶I. Petrovic, P. J. Heaney, and A. Navrotsky, *Phys. Chem. Miner.* **23**, 119 (1996).
- ⁴⁷D. R. Hamann, *Phys. Rev. Lett.* **76**, 660 (1996).
- ⁴⁸A. A. Demkov, J. Ortega, O. F. Sankey, and M. P. Grumbach, *Phys. Rev. B* **52**, 1618 (1995).
- ⁴⁹*Properties of Crystalline Silicon*, edited by R. Hull (Institute of Electrical Engineers, London, 1999).
- ⁵⁰D. R. Peacor, *Z. Kristallogr.* **138**, 274 (1973).
- ⁵¹N. R. Keskar and J. R. Chelikowsky, *Phys. Rev. B* **46**, 1 (1992).
- ⁵²G. Bersuker, J. Barnett, N. Moumen, B. Foran, C. D. Young, P. Lysaght, J. Peterson, B. H. Lee, P. M. Zeitzoff, and H. R. Huff, *Jpn. J. Appl. Phys., Part 1* **43**, 7899 (2004).